Prompt-γ production from 220 MeV/u ^{12}C ions interacting with a PMMA target

I. Mattei[c,g], F. Bellini[a,b], F. Bini[l], F. Collamati[a,b], E. De Lucia[c], M. Durante[f], R. Faccini[a,b], C. La Tessa[f], M. Marafini[b,e], S. Morganti[a,b], P. Ortega[i], R. Paramatti[a,b], L. Piersanti[c,d], M. Rovituso[f], A. Russomando[a,h], A. Sarti[c,d], C. Schuy[l], A. Sciubba[c,d], E. Solfaroli Camillocci[a], M. Vanstalle[f], C. Voena[a,b], V. Patera[c,d]

[a] Dipartimento di Fisica, Sapienza Università di Roma, Roma, Italy
[b] INFN Sezione di Roma, Roma, Italy
[c] Laboratori Nazionali di Frascati dell'INFN, Frascati, Italy
[d] Dipartimento di Scienze di Base e Applicate per Ingegneria, Sapienza Università di Roma, Roma, Italy
[e] Museo Storico della Fisica e Centro Studi e Ricerche "E. Fermi", Roma, Italy
[f] GSI, Darmstadt, Germany
[g] Dipartimento di Matematica e Fisica, Roma Tre Università di Roma, Roma, Italy
[h] Center for Life Nano Science@Sapienza, Istituto Italiano di Tecnologia, Roma, Italy
[i] CERN, Geneva, Swizterland
[l] Dipartimento di Ingegneria Meccanica e Aerospaziale, Sapienza Università di Roma, Roma, Italy

Abstract. The radiation used in hadrontherapy treatments interacts with the patient body producing secondary particles, either neutral or charged, that can be used to provide a fast feedback on the treatment plans.

Here, measurements of prompt photons particle fluxes produced by the interaction of a 220 MeV/u carbon ion beam at GSI, Darmstadt, with a polymethyl methacrylate (PMMA) target are reported at 60°, 90°, and 120° with respect to the primary beam direction. The photons were detected by means of a LYSO scintillator allowing for a measurement of time of flight and released energy. The detector experimental resolution is corrected for by means of an unfolding procedure tuned with a dedicated MonteCarlo simulation.

The spectra in the 2 – 10 MeV range are used to measure the integrated fluxes at 60°, 90° and 120°, yielding $\Phi_\gamma(60°) = (6.6\pm1.1) \times 10^{-3}$ sr^{-1}, $\Phi_\gamma(90°) = (7.4\pm1.3) \times 10^{-3}$ sr^{-1} and $\Phi_\gamma(120°) = (5.0\pm1.4) \times 10^{-3}$ sr^{-1} respectively.

PACS numbers:

Introduction

Presently, one of the major challenges in particle therapy is to provide a precise "in-treatment" monitoring of the irradiated volume position (Knopf and Lomax 2013). Nowadays, after a particle therapy treatment, a verification is accomplished with an in-situ Positron Emission Tomography (PET) which offers only an offline control on the released dose and is hence affected by uncertainties related to body motion and biological wash-out of the β^+ emitters. Several methods have been proposed as an alternative to the PET not only to improve its accuracy but also to include a real time check of the treatment planning delivered (Faccini and Patera 2015). All novel techniques are based on the correlation between the target volume position and the emission profile of secondary particles produced by nuclear interactions of the primary beam with the patient's body.

The yield of secondary charged and neutral fragments emitted at large angles (above 60 degrees with respect to the primary beam direction) by 220 MeV/u ^{12}C ions interacting with a polymethyl methacrylate (PMMA) target has been investigated. The results for secondary ions have been published (Piersanti et al. 2014). In this paper the kinetic energy spectra of prompt photons at several angles are reported, as well as the total integrated fluxes in the 2–10 MeV range.

Prompt photons are due to the nuclear de-excitation following the interaction of the impinging carbon ion with the nuclei of the target. In the past related measurements where made with carbon beams of 73 MeV/u (Testa et al 2008, Testa et al 2009) and 80 MeV/u (Agodi *et al* 2012a, Bellini *et al* 2013). In particular the latter measurement reported a prompt gamma rate at $90^\circ = (2.32 \pm 0.15) \times 10^{-3}$ sr^{-1}. The increase from these energies to 200 MeV/u implies an increase of range from about 1 cm to about 10 cm.

1. Experimental setup

The experiment was performed at the GSI laboratory (Darmstadt, Germany) where a 20×5×5 cm^3 PMMA target was exposed to a 220 MeV/u ^{12}C ion beam. The experimental setup, shown in Fig. 1, has been already described in detail in (Piersanti et al. 2014).

To detect the incoming carbon ions, two 1.1 mm thick plastic scintillators (StartCounter1, SC1 in the following, and StartCounter2, SC2 in the following) were placed at 37 cm and 16 cm respectively upstream of the PMMA target. Each detector, used for triggering and ion counting purposes, was read-out by two Hamamatsu 10580 photomultiplier tubes (PMTs). Both the start counters time and charge information were acquired, but only the one (SC2) closest to the PMMA was used to build the trigger, implemented as the OR of the two PMTs in coincidence with the LYSO detector signal.

A 10×10×0.2 cm^3 plastic scintillator (VETO in Fig. 1) was placed on the target side, before the drift chamber and LYSO detector array, to stop electrons with energy

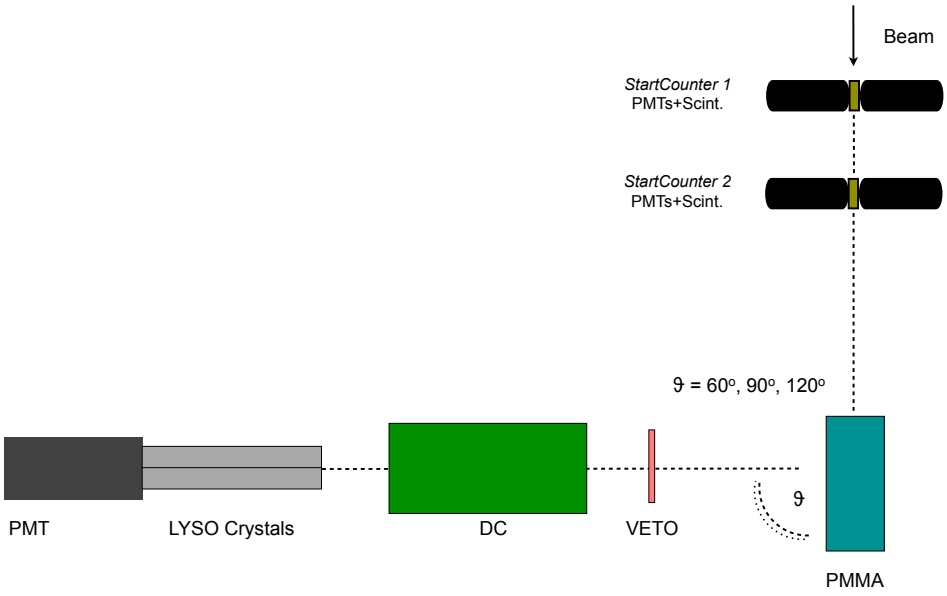

Figure 1. Scheme of the experimental setup (not to scale). The LYSO, DC and VETO detectors were fixed on a moving bar that was placed at different angles with respect to the beam axis, $\theta = [60, 90, 120]$ degrees, during the data acquisition.

$\lesssim 0.55$ MeV.

A 21 cm long Drift Chamber (DC), whose details are described in (Abou-Haidar *et al* 2012, Agodi *et al* 2012b, Piersanti *et al* 2013), was placed in front of the LYSO detector array at 41 cm from the target center and provided additional useful information to reject a possible background from secondary low energy prompt charged particles.

A scintillation detector (LYSO), composed of an array of 4 LYSO crystals, $1.5{\times}1.5{\times}12$ cm^3 each, was placed at a lateral distance of 65.8 cm from the target center for the detection of secondary particles. The scintillation light of the crystals was detected with an EMI 9814B PMT. The energy and time calibration of the LYSO crystals have been described in (Agodi *et al* 2012a, Bellini *et al* 2013).

The whole detector setup (LYSO, DC and VETO) was fixed on a moving arm that was placed at different angles with respect to the beam direction to study the angular distribution of the fragment yield. Three configurations have been studied: 60, 90 and 120 degrees.

The trigger signal was provided by the coincidence of the signals of the start counter closer to the PMMA target (SC2) and the LYSO detector within an 80 ns time window. The threshold used to discriminate the signal from the LYSO PMT was set to 130 mV. That threshold, expressed in terms of calibrated energy deposited in the LYSO crystal (E_{LYSO}), is equivalent to $\sim$1 MeV. The trigger rate was below 1 kHz when the primary beam particle rate was $\simeq$ 2 MHz.

The front-end electronics was read-out by a VME system (CAEN V2718 VME-PCI bridge) interfaced with a PC that acts as the Data AcQuisition (DAQ) server. The time and charge information for the signals of all the detectors were acquired using a 19-bit

TDC Multi-hit (CAEN V1190B, time resolution of ∼100 ps), and a 12-bit QDC (CAEN V792N, resolution of ∼0.1 pC).

The number of carbon ions (N_C) collected for a given data taking run was measured by counting with a scaler (CAEN V560 N) the number of events in which both PMTs of SC2 were giving a signal over threshold. Since the scaler allows for a maximum frequency for 100 MHz and the beam rate was well below that threshold, the scaler counts were considered as DAQ dead time (DT) free, and no DT correction was computed. Details on how N_C has been corrected in order to account for the event loss due to the signal discrimination implementation are given in § 3.

2. Prompt photon yields

When a ^{12}C ion interacts with the PMMA phantom, nuclear excitation can occur and *prompt photons* (photons with a very short emission time) can be generated by the de-excitation of the nuclei. The energy spectrum of the photons emitted from the PMMA was measured using the LYSO detector, and a detailed MC simulation has been used in order to take into account the detector efficiency and resolution effects when using the number of reconstructed photons (N_γ^{rec}) to compute the number of photons (N_γ) produced in the PMMA.

The energy deposition in the LYSO crystal ($\mathrm{E_{LYSO}}$) vs the Time of Flight (ToF) is studied to separate prompt photons from neutrons and other secondaries as, for example, charged particles. The ToF is computed as the time difference between the signal detected in the SC2 induced by a traversing carbon ion and the signal detected in the LYSO crystals ($T_{\mathrm{LYSO}} - T_{SC2}$). Note that we have not taken into account the time difference between the carbon ion interacting in the SC2 and its photon prompt emission in the PMMA (∼ 2 ns) when computing ToF. This is justified because we use it only for the prompt photons selection. The slewing effect induced by the front-end electronics fixed voltage threshold are instead accounted for as in (Agodi *et al* 2012a). The corrected quantity will be called ToF in the following. The analysis of the two dimensional $\mathrm{E_{LYSO}}$ vs ToF distribution allows an highly efficient selection of a pure sample of prompt photons.

The correlation between the measured energy $\mathrm{E_{LYSO}}$ and the ToF is shown in Fig. 2. The horizontal, low energy, band is due to the LYSO intrinsic noise, the almost vertical band at 0 ns is due to the signal from the prompt photons and the diffused cloud is mainly due to neutrons at ToF values larger than those of the prompt photons population. Moreover, it is visible an exponential-like band up to high energies (∼ 70 MeV), which represents secondary charged particles, mainly protons. A detailed view of the prompt photons region in the energy range 1-10 MeV is shown as an inset in Fig. 2.

To evaluate N_γ^{rec}, as already outlined in (Agodi *et al* 2012a), the time pull ($\mathrm{ToF}/\sigma_{\mathrm{ToF}}$) distribution, sampled in released energy bins, has been used. The number of reconstructed prompt photons in each energy bin was estimated from an unbinned

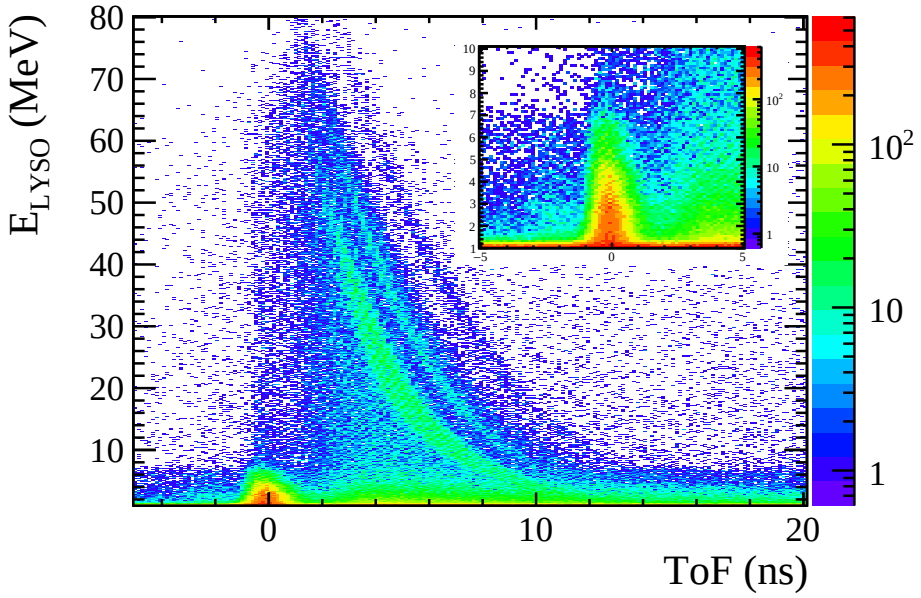

Figure 2. Energy deposition in the LYSO crystals as a function of ToF. The prompt photons, neutrons and charged particles populations are distinguishable as described in the text. The inset shows a zoom of the spectra in the range that is relevant for prompt photons.

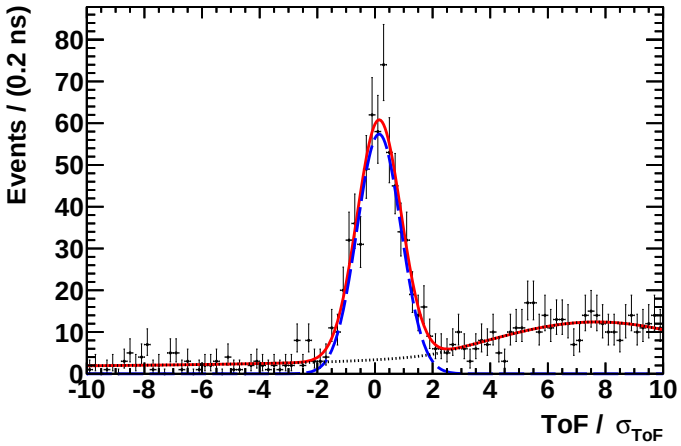

Figure 3. Example of ToF pull distribution in one energy slice (1.5 MeV < E <1.6 MeV). The dashed line indicates the gaussian fit to the signal; the dotted line indicates the Crystal Ball function that was used to model the neutron background.

maximum likelihood fit. Hence, N_γ^{rec} has been extracted from the extended likelihood fit to the ToF pull distribution for each energy slice. Fig. 3 shows an example of the pull distribution in the energy bin 1.5 MeV <E_{LYSO} <1.6 MeV, for one run in the experimental angular configuration at 90°. The total fit function is superimposed (red solid line): the background, mainly due to neutrons, is described by a Crystal Ball shape (Swarnicki 1986) and shown as a dotted line while the signal is modeled using a gaussian PDF (blue dashed line). The raw energy spectra measured for different angular

configurations are shown in Fig. 4 (left).

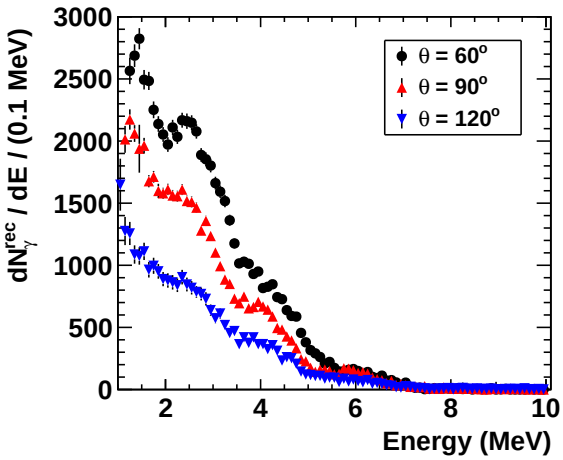

Figure 4. Energy spectra of prompt photons detected by the LYSO scintillator at 60° (circles), 90° (upward triangles) and 120° (downward triangles). These spectra are corrected for the DT efficiency (see § 3).

The measured photons spectra have to be corrected for the detector efficiencies and energy resolution, in order to have access to the true prompt photons production spectrum. The detector effects were taken into account by using an unfolding algorithm (Schmitt 2012) ‡. The algorithm was trained on the full FLUKA Monte Carlo (MC) simulation of the experiment, reproducing the geometric and physical characteristics of all the experimental setup components and including the observed light yield variations among the four LYSO crystals ($\sim$ 20%). For this training we used a MC sample comparable in size with data and uniformly distributed in energy.

The configuration of the TUnfold algorithm that was found to optimize the agreement of the unfolded spectrum with the true one in MC tests was the following: *kRegSize* scheme as regularization, 35 bins of the folded spectrum, and regularization strenght $\tau \sim 0.001$, with small variations related to the different sample statistics for the 60°, 90° and 120° analyses.

To asses the systematic error related to the unfolding procedure, the measured spectra have been unfolded with different parameters, varied within a range where similar agreement was obtained on the full simulation between unfolded and true spectrum. Also, as systematic check, the unfolding matrix was recomputed using the simulated energy spectrum as opposed to the flat one.

3. Prompt photon energy spectra

The prompt photons flux is defined in each energy bin E_i as:

$$\Phi_\gamma(E_i) = \frac{N_\gamma^i}{N_C \times \varepsilon_{DT} \times \varepsilon_{geo}} \quad (1)$$

‡ implemented in the ROOT TUnfold class

where N_C is the number of carbon ions impinging on the PMMA, ε_{DT} is the DT inefficiency, ε_{geo} is the detector geometrical acceptance and N_γ^i is the number of prompt photons measured from the unfolded spectrum in each energy bin.

The value of N_C measured with the scaler, needs to be corrected for the probability that more than one carbon ion interacts with the SC2 detector within the discrimination time of the SC2 signal (80 ns). In this time window the arrival of multiple carbon ions cannot be measured by the scaler resulting in an underestimation of the incoming ion total number. A detailed MC simulation of the beam rate and spill shape has been performed with FLUKA, allowing to compute the correction factor for the different beam rate conditions during the data taking. The simulation, validated against the measured beam shape and SC2 signal timing on data, yielded a correction factor of XXXX±YYY. The uncertainty accounts for both the statistical and systematic uncertainty, computed by varying the beam shape models and mean rate conditions.

The DT inefficiency ε_{DT} was computed using the instantaneous event by event rate measured during the data acquisitions as already presented in (Piersanti et al. 2014). In order to compute the loss of prompt photon events due to the DT, a study of the rate spectra has been performed. The rate in the $[0\ \mu s - 50\ \mu s]$ range, that was not accessible due to the DT, has been extrapolated using a fit in the $[50\ \mu s - 0.1\ s]$ range. ε_{DT} was hence measured as the fraction of events lost due to the acquisition dead time in the $[0\ \mu s - 50\ \mu s]$ time window, as known from the fit result. The measured values, varying from few % to 20%, showed the expected correlation with the carbon ion mean rates observed during the data acquisition time, varying from 100 kHz to few MHz. To take into account for maximal and minimal DT configurations, we assigned a systematic uncertainty to ε_{DT} by varying the fit model used to describe the rate spectra.
The detector geometrical acceptance (ε_{geo}) was calculated using the FLUKA *FULL* MC simulation sample.

Fig. 5 shows the unfolded prompt photons production flux as a function of the production energy for the 60° (full black circles), 90° (full up red triangles) and 120° (full down blue triangles) angular configurations. The errors are the sum in quadrature of all the contributions CAN WE QUANTIFY WHICH FRACTION IS CORRELATED AND WHICH UNCORRELATED? THEY LOOK MOSTLY CORRELATED. The uncertainty on ε_{geo}, computed using the *FULL* MC, gives a negligible contribution to the total systematic uncertainty.

The spectra are consistent among them, confirming the isotropic emission of prompt gamma. Consistently with previous measurements they end before $E_\gamma = 8$ MeV, confirming the fact that the They also show the 4.4 MeV and 6.1 MeV lines characteristic of ^{12}C and ^{16}O respectively. AND AROUND 3 MeV?

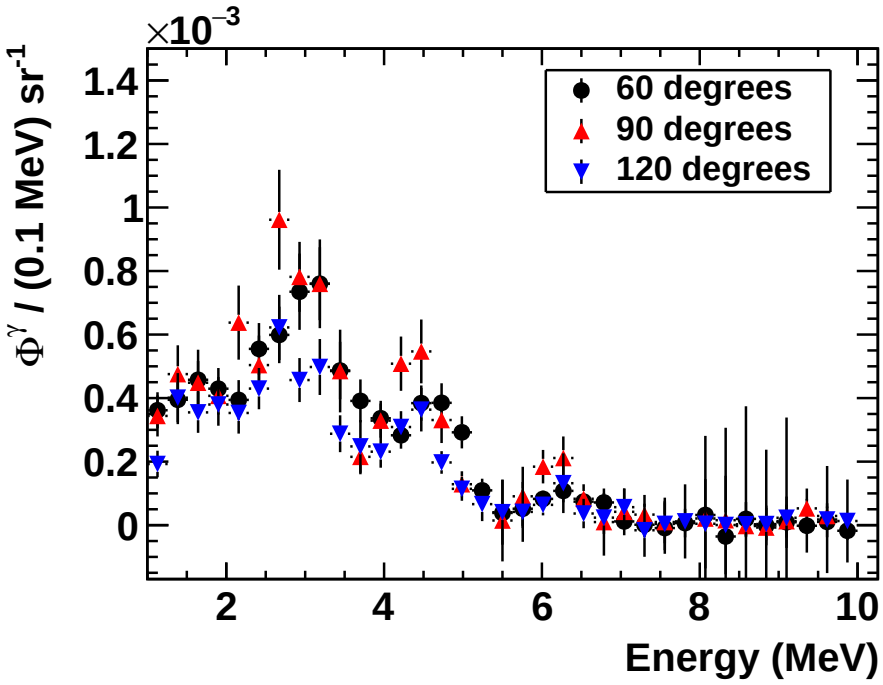

Figure 5. Unfolded energy spectra of prompt photons detected by the LYSO scintillator at 60° (circles), 90° (up triangles) and 120° (down triangles).

4. Prompt photon integrated rates

Besides the energy spectra, the produced prompt photons integrated flux is another interesting parameter that has to be precisely measured when developing photon detectors for dose monitoring applications (Agodi *et al* 2012a).
The photons production rates are defined as the energy integral of the spectra shown in Fig. 5 between 2 MeV and 10 MeV and are listed below for the 60°, 90° and 120° angle configurations:

$$\Phi_\gamma(E > 2 \text{ MeV } @60^\circ) = (6.59 \pm 0.22_{\text{stat}} \pm 1.07_{\text{sys}}) \times 10^{-3}\ sr^{-1}$$

$$\Phi_\gamma(E > 2 \text{ MeV } @90^\circ) = (7.39 \pm 0.38_{\text{stat}} \pm 1.27_{\text{sys}}) \times 10^{-3}\ sr^{-1}$$

$$\Phi_\gamma(E > 2 \text{ MeV } @120^\circ) = (5.02 \pm 0.24_{\text{stat}} \pm 1.34_{\text{sys}}) \times 10^{-3}\ sr^{-1}$$

The measurement uncertainties are dominated by the systematic contribution, that takes into accountcan we indicate an estimate of the relative contributions?:

- The limited knowledge of the DT efficiency correction: the systematic uncertainty has been computed assuming maximal and minimal DT configurations and recomputing the flux.
- The MC simulation used to build the unfolding matrix: the flux has been recomputed using the *FULL* simulation to produce the unfolding matrix, and the difference has been used to quote a systematic uncertainty.

- The choice of the unfolding parameters: the raw spectrum unfolding has been redone changing the regularization strenght within the stepping range used to scan the parameter phase when performing the unfolding tuning.

To cross check the result obtained with the FLUKA simulation software, the raw spectra unfolding has been redone using the Geant4 simulation (Agostinelli *et al* 2003, Allison *et al* 2006) to build the unfolding matrix. The change in the final result when using Geant4 is smaller than the systematic uncertainty already ascribed to the unfolding algorithm, and thus has not been accounted as a different contribution to the systematic uncertainty.

Another possibile systematic effect that has been evaluated is related to the possibility that a low energy charged particles contamination is present in the N_γ signal, evaluated from the ToF pull distributions. The Drift Chamber information has been used to recompute the fluxes while explicitly rejecting any charged particle, identified using the number of cells (N_{hits}) hit in the DC as discriminating variable. Charged particles were identified by the DC as events with $N_{hits} \geq 8$ with an efficiency of $\sim 98\%$ (Piersanti et al. 2014). We verified that there was a negligible change in the measured rate when including the $N_{hits} < 8$ requirement and hence no systematic uncertainty coming from the DC selection has been quoted.

Conclusions

A measurement of the prompt photons production rates and emission energy spectra was performed at the GSI facility using a ^{12}C beam of 220 MeV/u impinging on a PMMA phantom. Such measurements, performed at different angles with respect to the incoming beam direction, are key ingredients of any research and development strategy aiming for the construction of a dose monitor for particle therapy applications exploiting the secondary prompt photons produced inside the patient.

The result is in good agreement with what is expected from a similar measurement performed at a smaller beam energy (Agodi *et al* 2012a), where the photon production rate of a ^{12}C beam of 80 MeV/u was measured at 90° to be $(2.32 \pm 0.15) \times 10^{-3}$ sr^{-1}. The rate measured with a ^{12}C beam of 220 MeV/u, and reported here, is $(7.39 \pm 1.32) \times 10^{-3}$ sr^{-1}. As expected the higher energy beam produce a higher prompt photon flux than the lower one.

The results obtained at 60° and 120° are supporting the isotropic nature of the prompt photons production mechanism because they show a very good agreement with the measurements at 90°.

Aknowledgements

We would like to thank Marco Magi (SBAI Department) for his valuable help in the construction of the mechanical support This work has been partly supported by the "Museo storico della Fisica e Centro di studi e ricerche Enrico Fermi".

References

Z. Abou-Haidar, C. Agodi, M. Alvarez, M. Anelli, T. Aumann, *et al.*, "Performance of upstream interaction region detectors for the FIRST experiment at GSI," *JINST*, vol. 7, p. P02006, 2012.

C. Agodi *et al.*, "Precise measurement of prompt photon emission for carbon ion therapy," *JINST.*, vol. 7, p. 03001, 2012.

C. Agodi *et al.*, "Charged particle's flux measurement from PMMA irradiated by 80 MeV/u carbon ion beam," *Phys.Med.Biol.*, vol. 57, p. 5667, 2012.

C. Agodi *et al.*, "Study of the time and space distribution of beta+ emitters from 80 MeV/u carbon ion beam irradiation on PMMA," *Nucl. Instrum. Meth. B*, vol. 283, 2012.

S. Agostinelli *et al.*, "Geant4: a simulation toolkit," *NIM A*, vol. 506, no. 3, pp. 250-303, 2003.

J. Allison *et al.*, "Geant4 Developments and Applications," *IEEE Trans. Nucl. Sci.*, vol. 53, no. 1, pp. 270-278, 2006.

U. Amaldi and G. Kraft, "Radiotherapy with beams of carbon ions," *Rep. Prog. Phys*, vol. 68, p. 1861, 2005.

F. Attanasi *et al.*, "Comparison of two dedicated in beam PET systems via simultaneous imaging of ^{12}C-induced β^+-activity," *Phys.Med.Biol.*, vol. 54, p. 29, 2009.

F. Bellini *et al.*, "Extended calibration range for prompt photon emission in ion beam irradiation," *arXiv:* 1307.5689.

G. Battistoni, S. Muraro, P. R. Sala, F. Cerutti, A. Ferrari, *et al.*, "The FLUKA code *et al* Description and benchmarking," *AIP Conf.Proc.*, vol. 896, pp. 31–49, 2007.

M. Durante and J. Loeffler, "Charged particles in radiation oncology," *Nat. Rev. Clin. Oncol*, vol. 7, p. 37, 2010.

W. Enghardt *et al.*, "Charged hadron tumour therapy monitoring by means of PET," *Nucl. Instrum. Meth. A*, vol. 25, p. 284, 2004.

R. Faccini, V. Patera, "Dose Monitoring in Particle Therapy," accepted by Modern Physics Letters A, arXiv:??

A. Ferrari, P. Sala, A. Fassò, and J. Ranft, "FLUKA *et al* a multi particle transport code," *Tech. Rep. CERN-2005-10*, vol. INFN/TC05/11, 2005.

F. Fiedler *et al.*, "In-beam PET measurements of biological half-lives of ^{12}C irradiation induced β^+-activity," *Acta Oncol.*, vol. 47, p. 1077, 2008.

K. Gwosch *et al.*, "Non-invasive monitoring of therapeutic carbon ion beams in a homogeneous phantom by tracking of secondary ions," *Phys.Med.Biol.*, vol. 58, p. 3755, 2013.

P. Henriquet *et al.*, "Interaction vertex imaging (IVI) for carbon ion therapy monitoring *et al* a feasibility study," *Phys.Med.Biol.*, vol. 54, p. 4655, 2012.

O. Jakel, C. Karger, and D. Jurgen, "The future of heavy ion radiotherapy," *Med. Phys.*, vol. 35, p. 5653, 2008.

A. Knopf and A. Lomax, "In vivo proton range verification *et al* a review," *Phys.Med.Biol.*, vol. 58, pp. 131–160, 2013.

Y. Koba *et al.*, "Scintillation Efficiency of Inorganic Scintillators for Intermediate-Energy Charged Particles," *Prog. Nucl. Sci. Tech.*, vol. 1, p. 218, 2011.

C. Min, C. Hyeong Kim, M. Youn, and J. Kim, "Prompt gamma measurements for locating the dose falloff region in the proton therapy," *Appl. Phys. Lett.*, vol. 89, p. 183517, 2006.

K. Mosegaard and A. Tarantola, " Probabilistic Approach to Inverse Problems," *International Handbook of Earthquake & Engineering Seismology (Part A), Academic Press*, vol. 237, 2002.

K. Parodi, W. Enghardt, and T. Haberer, "In-beam PET measurements of β^+ radioactivity induced by proton beams," *Phys.Med.Biol.*, vol. 47, p. 21, 2002.

J. Pawelke *et al.*, "In-beam PET imaging for the control of heavy-ion tumour therapy," *IEEE Trans. Nucl. Sci.*, vol. 44, p. 1492, 1997.

L. Piersanti *et al.*, "Measurement of charged particle yields from PMMA irradiated by a 220 MeV/u 12C beam", *Phys.Med.Biol.*, vol. 59, p. 1857, 2014.

D. Schardt, T. Elsasser, and D. Schulz-Ertner, "Heavy-ion tumor therapy *et al* physical and radiobiological benefits," *Rev. Mod. Phys.*, vol. 82, p. 383, 2010.

S. Schmitt, "TUnfold: an algorithm for correcting migration effects in high energy physics," JINST 7 (2012) T10003 [arXiv:1205.6201]

T. Skwarnicki, "A study of the radiative CASCADE transitions between the and resonances," *'Tech. Rep.*, (1986).

E. Testa *et al.*, "Monitoring the Bragg peak location of 73 MeV/u carbon ions by means of prompt γ-ray measurements," *Appl. Phys. Lett.*, vol. 93, p. 093506, 2008.

E. Testa *et al.*, "Dose Profile monitoring with carbon ions by means of prompt-gamma measurements," *Nucl. Instrum. Meth. B*, vol. 267, p. 993, 2009.

S. Vecchio, F. Attanasi, N. Belcari, and M. Camarda, "A PET prototype for in-Beam monitoring of proton therapy," *IEEE Trans. Nucl. Sci.*, vol. 56, p. 1, 2009.

W. Verkerke, D. Kirkby, "The RooFit Toolkit for Data Modeling," *arXiv:physics/0306116*